Experiments in Fluids (2022) 63:34
https://doi.org/10.1007/s00348-021-03365-7

RESEARCH ARTICLE

Unstationary dynamics of drops subjected to MHz-surface acoustic waves modulated at low frequency

P. Brunet[1] · **M. Baudoin**[2]

Received: 2 August 2021 / Revised: 30 November 2021 / Accepted: 30 November 2021 / Published online: 24 January 2022

Abstract

In the present work, we investigate the unstationary dynamics of sessile droplets subjected to high-frequency surface acoustic waves modulated at a lower frequency close to the first inertio-capillary resonance mode of the drop. Under the action of both acoustic streaming and radiation pressure, the droplet response combines (i) a directional motion and (ii) oscillations of its shape and contact-line position. The droplet oscillations and time-averaged velocity show strong dependency on the modulation frequency. While the former dependence is linked to some resonance effects (harmonic and parametric), the latter one is still an unsolved issue. To get further insight of the underlying physics, we investigate here the fast oscillating dynamics of the drop contact line and of the dynamical contact angles through high-speed and high-resolution measurements at various modulation frequency. At odds with what is predicted and measured in stationary moving contact lines, we show that the contact-line velocity exhibits complex, non-single-valued dependence with the dynamic contact angles.

Graphical abstract

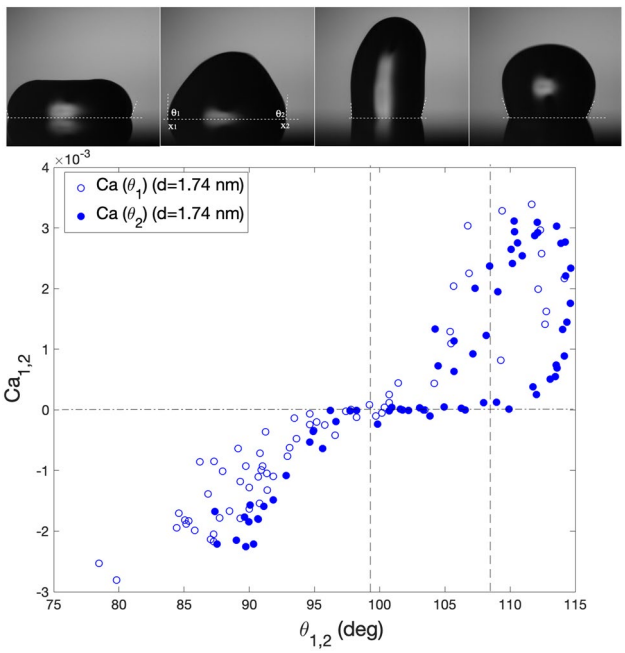

✉ P. Brunet
philippe.brunet@univ-paris-diderot.fr

Extended author information available on the last page of the article

1 Introduction

The motion of small amounts of liquids on substrates is often hindered by natural surface imperfections, which cause pinning force, generally quantified by a hysteresis in the contact angle (CA) adopted by the liquid droplet at the onset of advancing or receding motions (Bonn et al. 2009). This retention force is generally written as:

$$\mathcal{F}_R = a\gamma\pi R_0(\cos\theta_R - \cos\theta_A) \quad (1)$$

where γ is the surface tension between the liquid and the ambient, R_0 is the basal drop radius, a is a geometrical prefactor; θ_R and θ_A, respectively, stand for the static CA at the onset of the receding and the advancing motions, whose values are distinct from θ_Y the CA at thermodynamic equilibrium given by the Young's law. Mechanical vibrations prescribed to the substrate showed their ability to decrease or even cancel this retention force (Johnson and Dettre 1964; Andrieu et al. 1994; Decker and Garoff 1996; Della Volpe et al. 2002; Brunet et al. 2007), a phenomenon also measured in electrowetting (Li and Mugele 2008). The decrease in hysteresis could be related to the fact that vibrations make the contact line (CL) constantly unpinned (Noblin et al. 2004), allowing to jump over energy barriers caused by substrate imperfections (Long and Chen 2006). One of the key ingredients is to choose a vibration frequency close to that of the lowest modes of resonance of the drop (generally denoted as the Rayleigh-Lamb modes Lamb 1932). As the forcing frequency increases, the different modes of resonance of sessile drops were found to show more complex interplay between radial and azimuthal deformations (Bostwick and Steen 2014; Chang et al. 2015), offering a rich collection of spatial modes (Steen et al. 2019). To additionally induce a net directional motion of the drop, another key ingredient is to stimulate both the symmetric and asymmetric lower-frequency modes, which in practice is achieved either by combining horizontal and vertical vibrations with a phase shift (Noblin et al. 2009), or by prescribing slanted substrate vibrations (Brunet et al. 2007; Costalonga and Brunet 2020).

As an alternative to mechanical vibrations, and probably being a more versatile technique, surface acoustic waves (SAWs) of frequency above MHz are proven to be efficient in performing internal mixing, free-surface oscillations, jetting, splitting/merging and nebulisation of sessile droplets (Friend and Yeo 2011; Insepov et al. 2021; Lei and Hu 2020; Connacher et al. 2020). The droplet dynamics mainly results from the combination of two effects, namely acoustic streaming and radiation pressure (Brunet et al. 2010). While the former effect originates from the viscous dissipation of a leaky acoustic wave that propagates within the fluid and in turn generates a directional flow (Riaud et al. 2017), the latter one exerts a stress on the drop free surface (Chu and Apfel 1982; Cinbis et al. 1993; Elrod et al. 1989; Issenmann et al. 2008). For large enough acoustic power, the drop responds with a combination of large amplitude oscillations and net motion in the direction of the wave propagation in the solid (Brunet et al. 2010). The frequency of oscillations scales as $f_{osc} \simeq \alpha_r\left(\frac{\gamma}{\rho\mathcal{V}}\right)^{\frac{1}{2}}$ (Brunet et al. 2010), where ρ is the liquid density, $\mathcal{V}$ the drop volume and α_r a prefactor typically smaller than unity and whose exact value depends on the wetting properties (Tsamopoulos and Brown 1983; Strani and Sabetta 1984; Celestini and Kofman 2006; Bostwick and Steen 2009; Sharp 2012). For droplets of volume ranging between a few μl and 10 μl, f_{osc} is typically between 40 and 80 Hz and hence close to the lowest order symmetrical resonant mode (Lamb 1932). The discrepancy by several orders of magnitude between the high-frequency (MHz) excitation and the low-frequency response of the drop underlines a strongly nonlinear mechanisms that remain to be elucidated (Chastrette et al. 2021). The effect of the SAW frequency f_{ac} on the drop response, in particular its inner velocity, was investigated in several studies (Insepov et al. 2021; Alghane et al. 2012; Guo et al. 2014; Dentry et al. 2014; Shilton et al. 2014). A higher f_{ac} produces a more localised inner flow (Dentry et al. 2014; Shilton et al. 2014), but its effect on the drop motion is less obvious.

In a previous paper Baudoin et al. (2012), it was shown that modulations of the acoustic amplitude with a frequency f_m near the drop response frequency f_{osc} and near twice this frequency resulted in a strong increase of drop velocity (for the same acoustic power), respectively, corresponding to harmonic and parametric resonances. This strong coupling between free-surface or CL oscillations and translational velocity was confirmed in a later study for both sessile and pendant drops (Bussonniere et al. 2016), where a shift of response frequency with the amplitude of oscillations was measured and was found to be related to the averaged drop height. However, the dynamics at the CL level, which exhibits oscillations supposedly hindered by the pinning force from Eq. (1), was not investigated, although it should contain important clues for the understanding of the global (time-averaged) motion. Beyond these fundamental questions, to ease the motion of sessile droplets on substrates is a key issue in many applications, related to bio-fouling, surface cleaning or liquid droplet sorting on laboratory on chip (Bussonniere et al. 2021).

In the present study, we aim at improving the comprehension of the mechanisms behind this increase in velocity when modulation is prescribed near drop resonances, from the fast, local dynamics of the CL in SAW-actuated drops. Two possible scenarios are especially investigated:

1. Can the increase in velocity with amplitude of oscillations be attributed to a phase shift between droplet symmetric and asymmetric modes of oscillations ?
2. Can the increase in velocity be partly or totally attributed to a reduction or a shift of the CA hysteresis $\theta_A - \theta_R$ and then of $\mathcal{F}_R$? In other terms, could θ_A and θ_R be considered as velocity- or amplitude-dependent ?

We address these questions by carrying out experiments on sessile drops actuated with SAWs with frequency $f_{ac} \simeq 20$ MHz. The actuation here is modulated at a frequency f_m lying between 15 and 150 Hz, hence encompassing the first inertio-capillary eigenmodes of the drop. The modulation is used as a mean to study the influence of the oscillations on the drop global motion, as resonances phenomena lead to larger drop oscillations for the same injected acoustic power. Under the SAWs' excitation, the drop acquires an average velocity $\langle V \rangle$ and exhibits oscillations of its free-surface and basal radius, but not necessarily at the frequency of modulation f_m since superharmonic and subharmonic responses are observed. We recorded the dynamical contact angles θ_d and the position of the contact line along the substrate x versus time, with high-speed imaging and high spatial resolution. Related to the two aforementioned possible mechanisms, several previous investigations on oscillating CL dynamics reported measurements of θ_d versus instantaneous CL velocity V with non-single-valued dependence (Brunet et al. 2007; Ting and Perlin 1995; Jiang et al. 2004; Bradshaw and Billingham 2018). Such empirical laws clearly depart from Voinov's hydrodynamic theory of dynamical wetting (Voinov 1976) supposedly valid for stationary situations (Bonn et al. 2009; Dussan 1979; Petrov et al. 2003; Le Grand et al. 2005; Snoeijer and Andreotti 2013), or for weakly unstationary ones (Sikalo et al. 2005; Hodgson et al. 2021).

The paper is organised as follows: Section II presents the experimental setup, section III presents a qualitative description of the phenomena and introduces definitions of quantities relevant for averaged and fast dynamics analysis, section IV presents the quantitative results for both time-averaged and fast dynamics, and finally the results are discussed and synthesised in section V.

2 Experimental setup

The setup is similar to the one utilised in previous studies (Baudoin et al. 2012; Bussonniere et al. 2016): Sessile drops of deionised water are insonified by Rayleigh surface acoustic waves, generated on a 1.05-mm-thick (X-cut) lithium niobate ($LiNbO_3$) piezoelectric substrate. Interdigitated transducers (IDTs) are designed by successively sputtering a titanium (Ti) layer (20 nm thick) and a gold (Au) layer (200 nm thick) on the substrate. The SAWs are excited by a high frequency generator (IFR 2023A) and an amplifier (Empower RF 1037), see Fig. 1. Both the spacing and width of the interdigitated fingers (equal to $a = 43.75$ μm in the present system) determine the optimal frequency of the SAW according to the relationship $f_{\text{saw}} = c_s/\lambda = c_s/4a$ where λ is the wavelength and $c_s \approx 3484$ m.s^{-1} is the sound speed of Rayleigh waves. A f_{ac}=19.7 MHz excitation is used in this work as it maximises the drop response, a frequency which is close to the value $f_{saw} = 19.91$ MHz inferred from the acoustic properties of lithium niobate. The amplitude of the surface acoustic wave normal displacement d (characteristic of the wave magnitude) is measured with a Mach–Zehnder interferometer and found to range between 0.8 and 2 nm for a power suitable to induce both significant oscillations and net displacement of the drop. The signal prescribed on the IDT is modulated in amplitude, at a frequency $f_m \ll f_{ac}$ ranging typically between 15 and 150 Hz, hence close to the first droplet inertio-capillary eigenmodes. Hence, f_m is the main control parameter in our study. The acoustic frequency f_{ac} is kept at fixed value.

The substrate surface is treated by a self-assembled monolayer (SAM) of OTS (octadecyltricholorisilane) making it hydrophobic and with weak CA hysteresis. The advancing and receding angles, measured by successively inflating and deflating a sessile droplet at very low flow rate, are, respectively, $\theta_A = 108°$ and $\theta_R = 99°$. Reflections at the edge of the substrate are prevented by placing an acoustic absorber (Blu tack, UHU patafix) over the substrate contour and by adding a large liquid puddle (several ml) on the SAW path, behind the droplet. The droplet is actuated such that its net motion is always in the direction of the SAW propagation, so that no protection from unwanted liquid contact with the IDTs is required. To avoid chemical pollution on the surface, which would degrade the OTS treatment and would increase hysteresis after a few days, we carried out experiments in a class 1000 clean room. A droplet of volume $\mathcal{V} = 7.5$ μl is deposited on the substrate. The dynamics is recorded with a high-speed camera (Photron SA3). The typical frame rate used in our experiments is 2000 fps, in full frame (1 MP). We use powerful zoom with extension tubes to access the drop dynamics with high enough spatial resolution (4.07

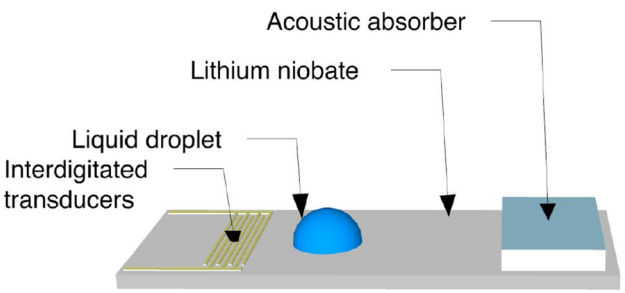

Fig. 1 Sketch of the experimental setup (see text for details)

μm per pixel). The best possible homogeneity in the field of the drop, suitable for extracting the drop motion and shape, is obtained with a cold continuous light pointed on a white screen at the background. Typical sequences are shown in Fig. 2, from which the horizontal position of drop CL at the left x_1 and right x_2 ends is extracted, as well as the corresponding CAs θ_1 and θ_2. These dynamical angles were measured from a linear extrapolation of the drop shape in the vicinity of the free-surface, after filtering, binarisation and outlining routines applied to the different sequences. This extrapolation was determined along a width of 20 pixels (corresponding to 82 μm), but we checked that the results on the angles were roughly the same if the width was chosen up to 50 pixels. Above this width, the drop shape can significantly departs from a straight wedge.

3 Definitions and phenomenological description

A first observation of the drop dynamics (see a typical example in Fig. 2) shows that the drop experiences a succession of stretching and spreading phases, where x_i and θ_i vary in a non-monotonous way and in many situations in a complex manner. Furthermore, during one cycle of oscillations, the values of both θ_i are comprised between θ_R and θ_A, in which the contact line is supposed to be pinned but also further below and beyond these values. It is important to understand what are the main forces that govern such an unstationary dynamics. In the classical stationary situation (see eg. Dussan 1979; Petrov et al. 2003; Le Grand et al. 2005), the spreading and dewetting of liquids on substrates are ruled by a balance between surface tension forces and viscous shear. The retention force due to substrate imperfections (eq. (1)) is generally considered as a constant in static and dynamical situations, and ruling the onset of motion (Bonn et al. 2009; Snoeijer and Andreotti 2013). The classical situations are those of a drop sliding on an incline plane, an immersed plate drawn out or dipped in a bath ("dip-coating") or a liquid plug moving along a capillary tube. The inner flow and free-surface shape generally reach a steady state, leading to a selection of dynamical contact angles θ_d given by the Cox–Voinov's law (Bonn et al. 2009; Snoeijer and Andreotti 2013):

$$\theta_d^3 - \theta_s^3 = 9\frac{\eta U}{\gamma}\log\left(\frac{\mathcal{L}_M}{l_m}\right), \tag{2}$$

where U is the contact-line velocity and η the dynamical viscosity. This relationship reflects the so-called viscous bending effect, occurring when $\mathrm{Ca} = \eta U/\gamma$ is large enough (typically $\geq 10^{-5}$) (Petrov et al. 2003; Le Grand et al. 2005). The dynamical angle θ_d is considered either at the front or the back of the drop, depending on the sign of U. The static angle θ_s is within the range of hysteresis $[\theta_R, \theta_A]$, and it was shown that θ_s should be equal, respectively, to θ_R or θ_A for receding or advancing contact lines (Petrov et al. 2003; Le Grand et al. 2005). Finally, $\mathcal{L}_M$ and l_m are, respectively, the macroscopic and microscopic (molecular) length scales. The model, that assumes a liquid free-surface of slowly varying slope, can be refined by including local variations of the slope or by combining it with other effects including mesoscopic slip length, the existence of a precursor film due to disjoining pressure or thermally activated jumps at molecular scale (Bonn et al. 2009; Snoeijer and Andreotti 2013). The latter effect has recently received specific attention, and its relevance was evidenced for very-low-hysteresis substrates ($< 2°$) (Perrin et al. 2016, 2018).

To what extent Eq. (2) remains valid if fluid inertia is not negligible anymore? This situation can occur in various situations, like during the first steps of wetting (Sikalo et al. 2005; Eddi et al. 2013), in a drop sliding on an inclined plate at high enough velocity (Hodgson et al. 2021; Puthenveettil et al. 2013), in interaction with a wake in a boundary-layer flow (Burgmann et al. 2021) or in liquid menisci or droplets subjected to oscillating forces from a vibrating substrate (Brunet et al. 2007; Ting and Perlin 1995; Jiang et al. 2004; Bradshaw and Billingham 2018; Hocking 1987; Miles

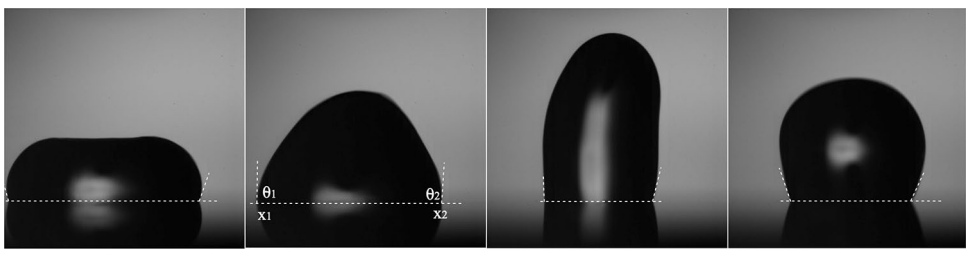

Fig. 2 Successive shapes taken by a sessile drop excited by $f_{ac} = 19.7$ MHz surface acoustic waves (SAWs) modulated at $f_m = 50$ Hz. The drop response combines both directional motion to the right (the direction of SAWs propagation) and free-surface oscillations. From high-resolution images, both the positions of the rear (left) and front (right) of the contact line are extracted (x_1 and x_2) as well as the corresponding dynamical contact-angles θ_1 and θ_2, indicated on one of the frames

1990). Our study comes with the scope of this latter situation. Historically, the influence of periodic shaking on drops or menisci has been partly motivated by the potentiality to induce a directional motion and to overcome the pinning forces due to substrate imperfections (Brunet et al. 2007; Noblin et al. 2009; Costalonga and Brunet 2020; Ting and Perlin 1995). Indeed, it was shown that such vibrations could partly or fully remove the pinning forces (Johnson and Dettre 1964; Andrieu et al. 1994; Decker and Garoff 1996; Della Volpe et al. 2002; Brunet et al. 2007; Li and Mugele 2008) on a rough and chemically inhomogeneous substrate. The decrease of hysteresis is related to that vibrations make the contact line constantly unpinned (Noblin et al. 2004) and susceptible to jump over energy barriers caused by the substrate imperfections (Long and Chen 2006). One generally obtains a hysteretic behaviour with a non-single-valued CL velocity $U(t) = \dot{x}_i$ versus θ_d, here $= \theta_i$, which clearly departs from Eq. (2) (Brunet et al. 2007; Ting and Perlin 1995; Bradshaw and Billingham 2018). Therefore, a question arising is how to explain and quantify this hysteretic behaviour and which ingredients have to be added in the dynamics to include the influence of fluid inertia ? Various studies have tried to address this question. One of the approaches consists in prescribing ad hoc conditions, which relate the instantaneous contact-line velocity and the macroscopic deformation at the vicinity of the contact line, as stated, for instance, in Hocking (1987), Fayzrakhmanova and Straube (2009). Another experimental study proposed a macroscopic effective slip length, which increases with the amplitude of oscillations (Ting and Perlin 1995). Other approaches attempt to solve the full hydrodynamics, which lead to a contribution of inertia involving Reynolds number-dependent terms (Cox 1998, Hocking and Davis (2002)). Without entering into such complexities here, the main reason why Voinov's framework and Eq. (2) fail in predicting the fast dynamics of oscillating CLs, should be that the corresponding inner visco-capillary flow does not reach a stationary regime. Instead, an unstationary boundary layer develops, with typical thickness $\delta = \left(\frac{2\eta}{\rho f_{osc}}\right)^{1/2}$, where f_{osc} is the typical frequency of the drop oscillations, and this layer can be significantly thinner than the drop height. Still, experiments on drops subjected to mechanical vibrations on a substrate showed that a relationship similar to eq. (2) could exist between the *time-averaged* dynamical angles and velocities, at least at an empirical level (Brunet et al. 2007, Costalonga and Brunet 2020).

The instantaneous unbalanced Young force per unit length of contact line (Bonn et al. 2009) is usually expressed as $\gamma(\cos\theta_i - \cos\theta_e)$, where $i = 1$ or 2 depending whether the left or the right side of the drop is considered, and $\theta_e = \theta_A$ or θ_R depending whether the contact line is in advancing or receding situation. When considering the whole drop, one should add the contribution of the whole contour, which can have a complex tridimensional shape. This issue is somewhat avoided if one considers that the spatial distribution of the CA can be simplified by taking two distinct values at the rear and the front sides (Dimitrakopoulos and Higdon 1998). Therefore, the problem finds a two-dimensional equivalent, and the resulting motile force on the drop at a time t is:

$$F_M(t) = 2\gamma\pi(\cos\theta_1 - \cos\theta_2)(x_2 - x_1) \tag{3}$$

where the term $(x_2 - x_1)$ accounts for the variations of the basal radius. The values of this radius $R(t)$ range between R_{min} and R_{max} over one period. Another important quantity is the width of this range ΔR:

$$\Delta R = R_{max} - R_{min} \tag{4}$$

which then quantifies the amplitude of CL oscillations. When integrated over a period of modulation $T_m = \frac{1}{f_m}$, it reads (Brunet et al. 2007):

$$\mathcal{F}_M = \frac{1}{T_m}\int_0^{T_m} \pi\gamma(\cos\theta_2 - \cos\theta_1)(x_2 - x_1)dt \tag{5}$$

Therefore, $\mathcal{F}_M$ is expected to be related to the averaged velocity $\langle V\rangle$ and possibly to ΔR. In practice, $\langle V\rangle$ is extracted from the mean displacement of the back-and-forth CL position over several (between 2 and 10) periods of oscillations. The equivalent dimensionless instantaneous velocity is the time derivative of the left and right CL positions:

$$\mathrm{Ca}_i = \frac{\eta\dot{x}_i}{\gamma}, \tag{6}$$

which are expected be related to θ_i. In what follows, we present results for both time-averaged and fast dynamics of CLs. We exploit that $\langle V\rangle$ and ΔR are strongly dependent on f_m (Baudoin et al. 2012) to extract x_i and θ_i for different values of f_m. From analysis of the fast dynamics, we expect to better understand the mechanisms behind this strong dependence. Since positive values for Ca_i correspond to an advancing situation, one takes the opposite of $\dot{x}_1$ in Eq. (6).

4 Results

4.1 Averaged dynamics: oscillations and directional motion

We first present results extracted from time-averaged quantities. The averaged velocity $\langle V\rangle$ and the maximal difference of basal radius ΔR are extracted for all values of f_m from 15 to 150 Hz, keeping the acoustic displacement constant, $d = 1.38$ nm. Figure 3-a presents the quantity $\Delta R \times f_m$, as a characteristic oscillation velocity for the contact line, versus

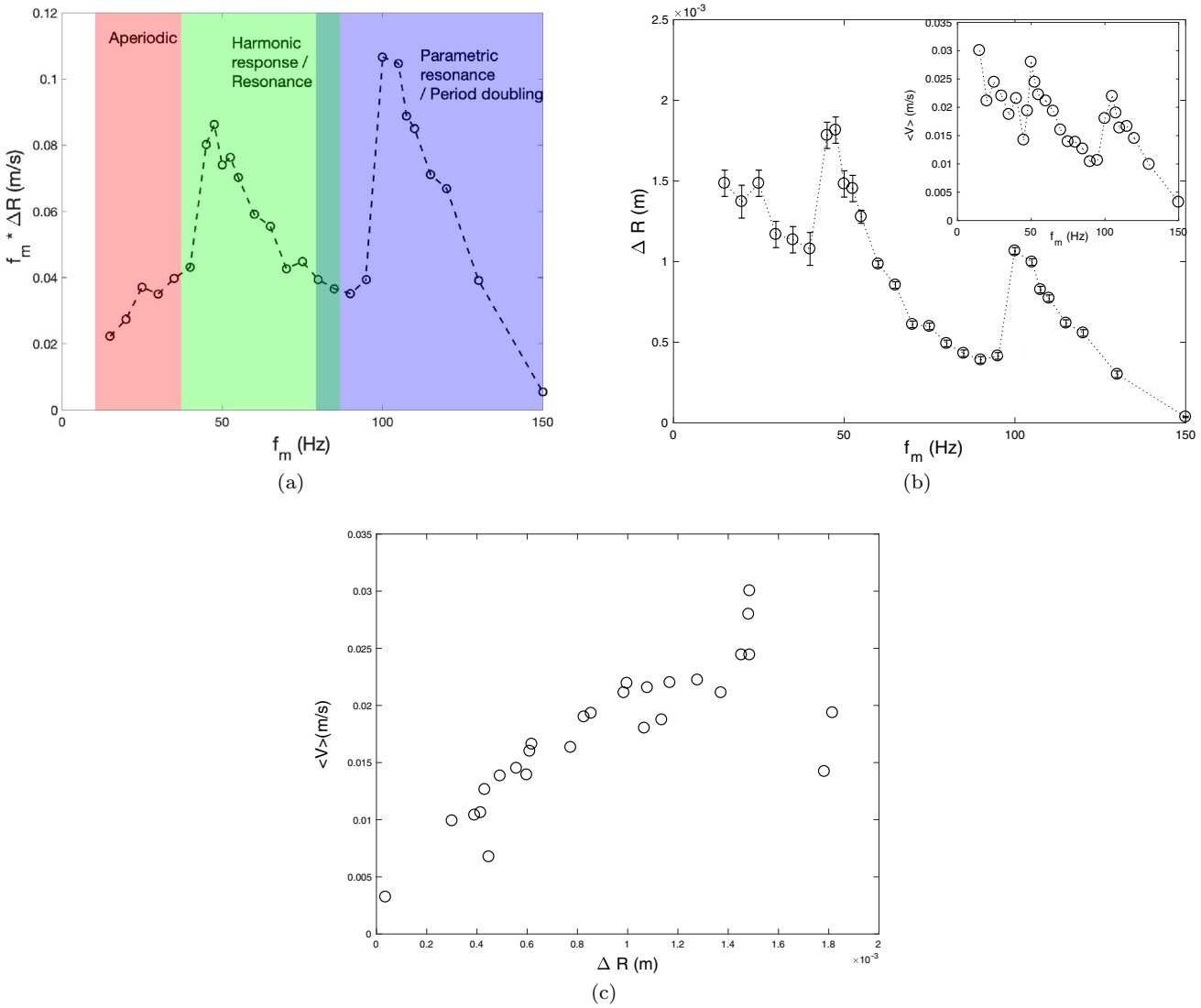

Fig. 3 Time-averaged dynamics of a SAW-driven droplet with various modulation frequencies f_m for an acoustic amplitude $d = 1.38$ nm. **a** Characteristic contact-line oscillation velocity $\Delta R \times f_m$ versus modulation frequency f_m. Coloured domains indicate the different regimes of response: aperiodic, harmonic (with or without resonance), period-doubling, period-doubling with parametric instability. **b** Basal radius difference $\Delta R = R_{max} - R_{min}$ versus f_m. Insert: corresponding averaged drop velocity $\langle V \rangle$. **c** Averaged drop velocity $\langle V \rangle$ versus ΔR

f_m, together with the frequency domains of the different responses of the drop contact line. These regimes are categorised into: aperiodic, quasi-harmonic, harmonic (with or without resonance), period-doubling, period-doubling with parametric instability. In practice, due to the variety in the drop responses, the averaging is done over several periods *of the drop response*, and not over periods of excitation. Figure 3-b shows ΔR versus f_m. Both these plots confirm the trends already reported in Baudoin et al. (2012). A clear maximum of amplitude of the CL oscillations is observed for $f_{max} \simeq 50$ Hz, while another local maximum appears at $\sim 2f_{max}$.

Figure 3-c plots $\langle V \rangle$ versus ΔR, showing a global increase, consistent with previous measurements (Baudoin et al. 2012; Bussonniere et al. 2016), except for the highest values of ΔR where a saturation phenomenon appears. The two data points at $\Delta R \simeq 1.8$ mm correspond to $f_m = 47.5$ Hz and 50 Hz, for which the drop does enter in resonance.

Following the results of previous studies (Brunet et al. 2007; Costalonga and Brunet 2020), where the averaged velocity of vibrating droplets was linearly dependent to the time integration of the motile force F_M, we plot the time-averaged value of F_M (see Eq. (5)) versus the dimensionless-averaged velocity $\langle \mathrm{Ca} \rangle = \frac{\eta \langle V \rangle}{\gamma}$, see Fig. 4-a. However,

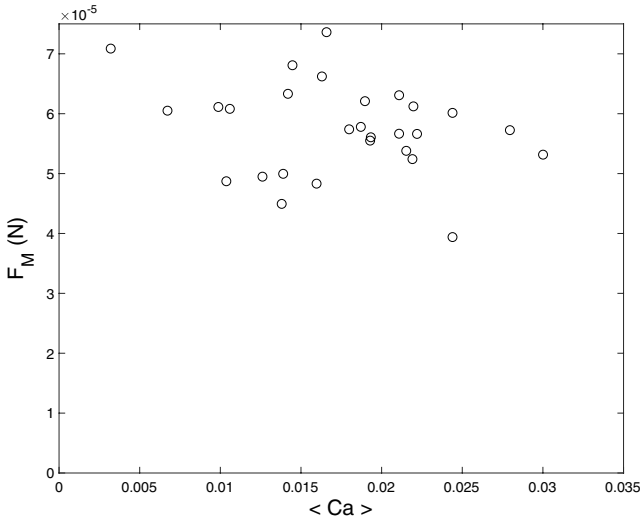

Fig. 4 **a** Averaged motile force (eq. (5)), based on dynamical angles in out-of-equilibrium situation, versus averaged dimensionless velocity $\langle Ca \rangle$ **b** dimensionless fraction of time (over one period) during which the left and right CAs are bounded between θ_R and θ_A (p_{CA}), and during which the left and right CLs are static (p_{CL}), versus maximal contact-line speed $\Delta R * f_m$

the averaged motile force does not show any clear trend with Ca: it remains bounded in a range between 45 and 70 μN. As a comparison, the retention force based on CA hysteresis calculated from Eq. (1) roughly equals $\mathcal{F}_R = 40$ μN.

We also examine whether or not a significant decrease in CA hysteresis can be evidenced, as it was observed for drops on mechanically vibrating substrates (Andrieu et al. 1994; Decker and Garoff 1996; Brunet et al. 2007), where the dynamics of CLs was shown to oscillate without any stop-and-go in the range of CA $\theta_R < \theta_i < \theta_A$. A first coarse attempt to address this point quantitatively is to determine the ratio of time (determined over a few periods) during which the contact line remains static: p_{CL}. The criterion to remain static is taken such as the positions x_i (i=1,2) vary by less than 1 pixel (about 4 microns) during the time interval between two frames 0.5 ms, leading to a velocity $\dot{x}_i$ smaller than 8 mm/s or a Ca_i roughly inferior to 10^{-4}. For the same measurements, we also determine the ratio of time p_{CA} during which θ_i is bounded between θ_R and θ_A. The results are plotted versus a characteristic CL oscillation velocity, here taken equal to $\Delta R * f_m$, see Fig. 4-b. While the calculation of these ratios is carried out on both θ_1 and θ_2, both the front and back sides show roughly the same trend. One notices a global decrease of p_{CA} and p_{CL} with $\Delta R * f_m$, but with some significant dispersion.

4.2 Local contact-line dynamics

We now focus on the fast, local CL dynamics. We computed the dimensionless velocities of the rear (left) and front (right) CLs over several periods of oscillations: Ca_1 and Ca_2 correspond, respectively, to the dimensionless velocity of horizontal coordinates x_1 and x_2, following the definition given in Eq. (6). We first prescribe $f_m = 50$ Hz, for which the drop response is close to the harmonic resonance and corresponds to a relatively large velocity. We prescribe various levels of acoustic power, quantified by the amplitude d. Figures 5-a–c present Ca_i versus θ_i ($i = 1$ and 2, respectively, for left and right CLs), at different values of d. Figure 5-d gathers all data for the three values of d for the sake of comparison.

The evolution of Ca_i with θ_i shows a non-trivial dependence, which clearly departs from the classical Cox–Voinov equation. Instead, and consistently with previous experiments in oscillating CLs (Ting and Perlin 1995; Jiang et al. 2004; Brunet et al. 2007; Bradshaw and Billingham 2018), Ca_i is not a single-valued function of θ_i and seems to depend on which phase of oscillation is considered. To further investigate the CL/CA dynamics in a more quantitative way, we opted to operate at fixed $d = 1.38$ nm and to vary f_m from 15 to 150 Hz. The choice for an intermediate value of acoustic amplitude d is motivated by that for too small values of d; the range of Ca_i is too narrow (roughly between -1.5×10^{-3} and 2.5×10^{-3}, see Fig. 5-a), while for too high values of d the dynamics of CLs becomes too much erratic.

Based on previous investigations on drops on mechanically vibrated substrates (Brunet et al. 2007; Noblin et al. 2009; Costalonga and Brunet 2020; Sartori et al. 2015, 2019), we focus on the relative contribution and phase shift between symmetric and asymmetric modes. The pumping (symmetric) mode can be quantified by the basal radius

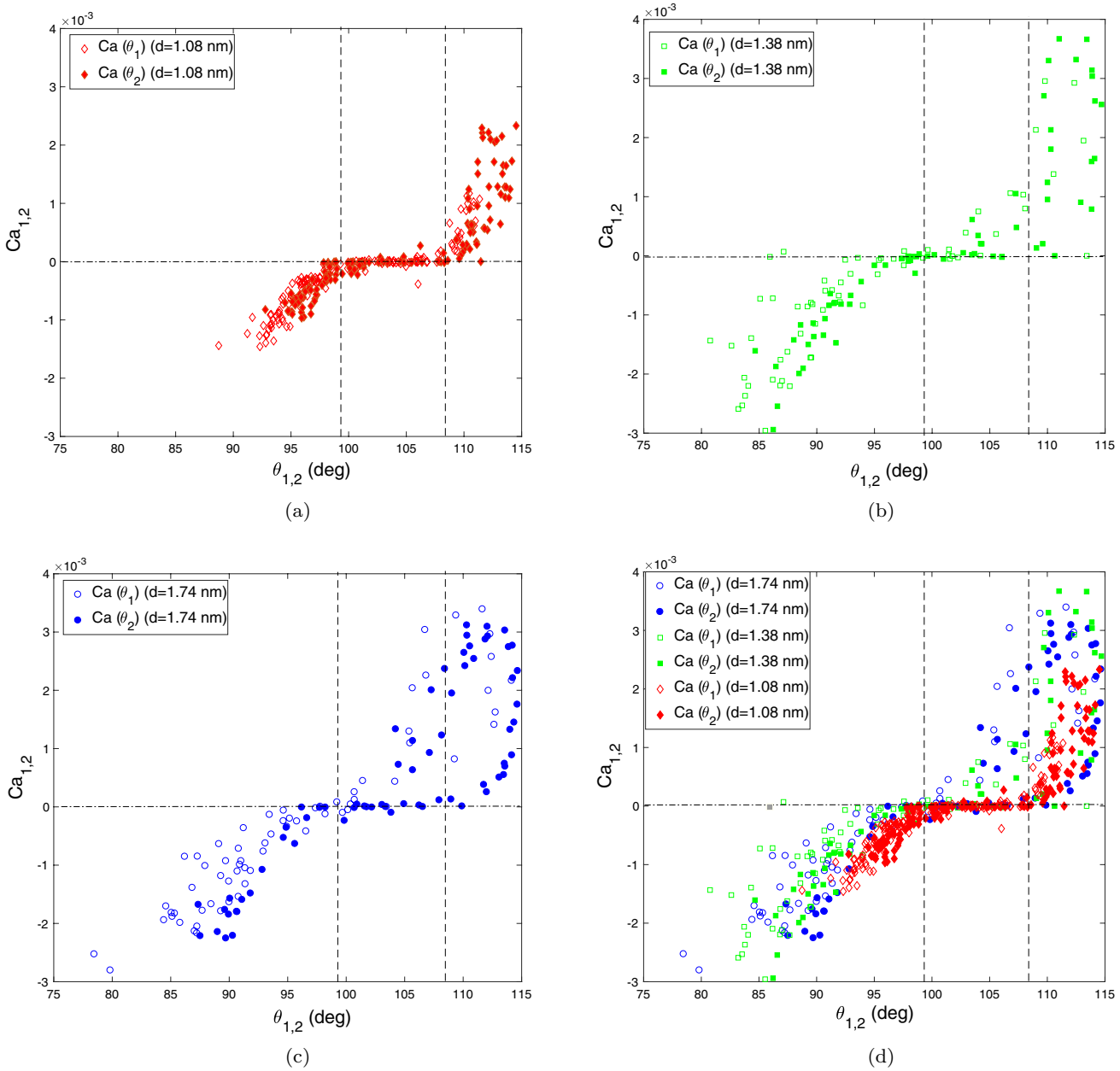

Fig. 5 Relationship between dynamical CA and dimensionless CL velocity at the rear/left (index 1, open symbols) and front/right (index 2, filled symbols) for a 7.5 μl drop excited by 19.7 MHz SAWs modulated at $f_m = 50$ Hz, at different acoustic powers. **a** $d = 1.08$ nm, **b** $d = 1.38$ nm, **c** $d = 1.74$ nm, **d** gathering of the three sets of data of (**a**, **b**, **c**). The horizontal dash-dotted line indicates static CLs, while the two vertical dashed lines show the values of static θ_R and θ_A

$R(t) = x_2 - x_1$, and the rocking (asymmetric) mode by the difference $(\cos\theta_2 - \cos\theta_1)$. Figures 6-a–f show these quantities over several periods with increasing f_m from (a) to (f). They illustrate in more detail the CL dynamics corresponding to the regimes mentioned in Fig. 3-a. One of the interesting behaviours is that the basal radius responds harmonically with the modulation f_m only within a reduced range of f_m (here roughly between 42 and 75 Hz) and that this situation corresponds to the largest amplitude ΔR (subfigure c), see also Fig. 3-b.

Below this range, $R(t)$ responds with a more complex behaviour, which actually depends whether f_m is compatible with the range of natural frequencies f_{osc} that the drop adopts. For instance, at f_m=30 Hz (subfigure (a)), the drop responds at a frequency f_{osc} slightly smaller than f_m (as

shown by the double-arrow representing $1/f_m$, shorter than the natural period the drop tries to adopt), with a combination of modes resulting in a non-periodic dynamics. At f_m = 25 Hz (non-represented), the drop responds almost harmonically, probably because it is near half the resonance frequency. At f_m=40 Hz (subfigure (b)), the response of the drop, although seemingly resulting from a combination of at least two modes, becomes closer and closer from a harmonic one, and slightly higher 40 Hz, the dynamics becomes progressively periodic. Just above 60 Hz, the basal radius shows the lowest amplitude of oscillations. When one increases f_m further, the drop still keeps low-amplitude response and exhibits period-doubling (subfigure (d)), which is identified as a progressive appearance of a parametric response (Baudoin et al. 2012). As f_m reaches roughly 100 Hz and above, the parametric response becomes dominant over the harmonic one, and the amplitude of drop oscillations experiences a sudden increase (see Fig. 3-a,b), which corresponds to subfigures (e,f).

It is important to check whether the maxima of the unbalanced capillary force, proportional to $(\cos\theta_2 - \cos\theta_1)$, correspond to minimal values of $R(t)$. In this prospect, the trends are less clear, especially at $f_m < 45$ Hz (a,b), where $(\cos\theta_2 - \cos\theta_1)$ can take strongly fluctuating values alternatively negative and positive. The net motion of the drop is somewhat limited by this. However, the dynamics for f_m = 55 Hz (subfigure (c)) clearly shows that the occurrences of high $(\cos\theta_2 - \cos\theta_1)$ correspond to the smallest values of $R(t)$, which promotes a net motion to the right direction. This feature is also observed to a certain degree for $f_m = 105$ and 107.5 Hz (e,f). For $f_m = 80$ Hz, the relatively slow net motion can be explained by the fact that $(\cos\theta_2 - \cos\theta_1)$ remains small : the drop left-right asymmetry remains weak. Therefore, at least some cases with relatively high $\langle V \rangle$ could find an explanation through the occurrence of phase opposition between $(\cos\theta_2 - \cos\theta_1)$ and $x_2 - x_1$, consistent with recent evidences on the role of phase shift in the motion of vibrating droplets on slippery substrates (Sartori et al. 2019), as well as with previous ones on surfaces with larger friction (Noblin et al. 2009).

However, the lack of trend of $\mathcal{F}_M$ with Ca in the determination of the time-averaged dynamics (Fig. 4-a) casts some doubts on a mechanism that would simply rely on the phase shift between $(\cos\theta_2 - \cos\theta_1)$ and $x_2 - x_1$. This point remains to be understood in detail.

From Fig. 5, we deduce that the relationship between instantaneous CL dimensionless velocities Ca_i and corresponding dynamical angles θ_i would reflect an unsteady dynamics. We now investigate the influence of f_m on this empirical relationship, at fixed amplitude d = 1.38 nm. The results are depicted in Fig. 7-a–d for four main different situations: (a) $f_m = 30$ Hz (aperiodic, erratic response with dominant f_{osc} close to f_m), (b) $f_m = 50$ Hz (resonant harmonic response, with the largest amplitude), (c) f_m = 95 Hz (small amplitude response with period-doubling, and (d) $f_m = 105$ Hz (large amplitude response with parametric instability and period-doubling). All the four plots show a certain degree of departure from classical stationary situations generally captured by Eq. (2): (i) in the sense that Ca_i takes at least two distinct values for the same θ_i, in either advancing or receding phases of the CL, (ii) in the sense that $\mathrm{Ca}_1(\theta_1)$ and $\mathrm{Ca}_2(\theta_2)$ take values which are shifted from each other. At 30 Hz, the left CL (open symbols) and right CL (filled symbols) describe distinct range of values. That for $(\theta_1, \mathrm{Ca}_1)$ is clearly shifted compared to that for $(\theta_2, \mathrm{Ca}_2)$. From direct visualisations of the sequences, we attribute this behaviour to a significant asymmetry of the drop over the whole period of oscillation, which could be enhanced by the influence of gravity, given that the drop height can be significantly larger than the initial one $h_0 \simeq R_0$ (see also Bussonniere et al. 2016). At 50 Hz, Ca_1, Ca_2 and θ_1, θ_2 roughly describe the same range of values. A remarkable feature is that the relationship $\mathrm{Ca}_i(\theta_i)$ follows a wide single loop, corresponding to the advancing and receding phases, which is observed in the whole range of harmonic resonance (47 to 55 Hz). At 95 Hz, the trend seems comparable to the previous one, but with a lesser extent for the range of values, and multiple and lesser defined loops with narrower width in the region of high CA. At 105 Hz, a shift between $(\theta_1, \mathrm{Ca}_1)$ and $(\theta_2, \mathrm{Ca}_2)$ is again noticed in the range of high CA and also with multiple narrow loops for each $(\theta_i, \mathrm{Ca}_i)$.

For all values of f_m, the instantaneous velocities taken within the range $[\theta_R, \theta_A]$—indicated by the interval between the two vertical dashed lines—strongly depart from a stationary situation, for which $[\theta_R, \theta_A]$ is defined as the range of static CL. The range of static hysteresis clearly does not hold in our experiments, since Ca_i takes significantly positive values within this range, and also as Ca_i can remain close to zero below this range.

5 Discussion and conclusions

Originating from an interplay between internal acoustic streaming and radiation pressure at the free surface, drops subjected to SAWs exhibit a combination of left–right asymmetry on their free surface with periodic oscillations of the basal radius, providing the acoustic amplitude d is large enough. This leads to a time-averaged net motion, with large-amplitude oscillations which enable the constant depinning of the CL. This dynamics can be enhanced by a modulation of the forcing acoustic amplitude at frequency f_m, taken in the same range as f_{osc}, the

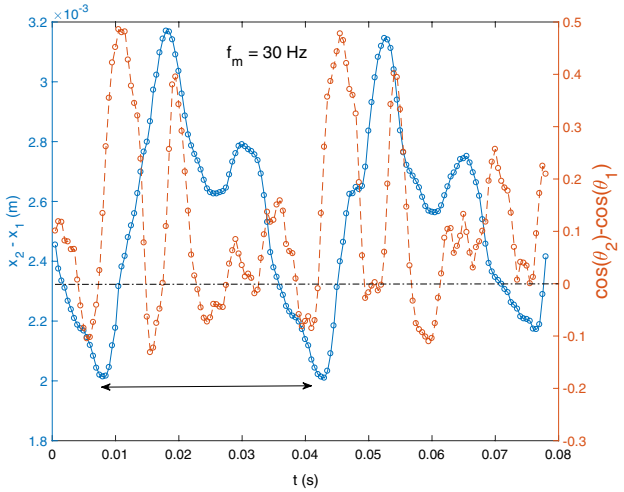
f_m = 30 Hz
x_2 - x_1 (m)
cos(θ_2)-cos(θ_1)
t (s)

(a)

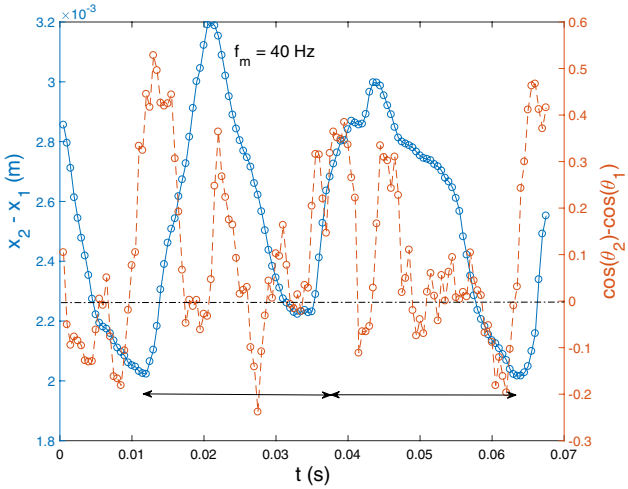
f_m = 40 Hz
x_2 - x_1 (m)
cos(θ_2)-cos(θ_1)
t (s)

(b)

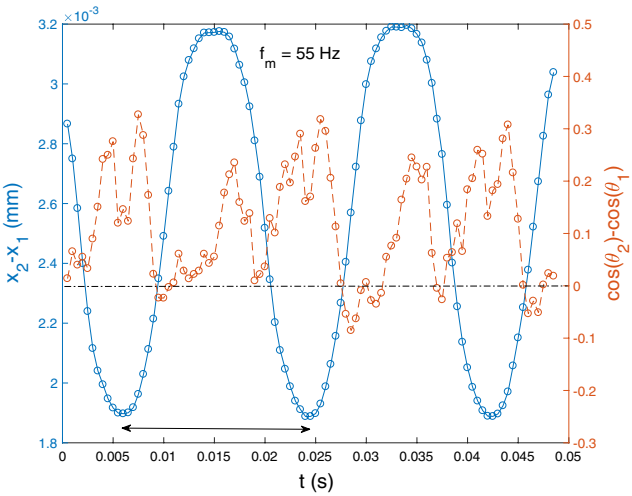
f_m = 55 Hz
x_2-x_1 (mm)
cos(θ_2)-cos(θ_1)
t (s)

(c)

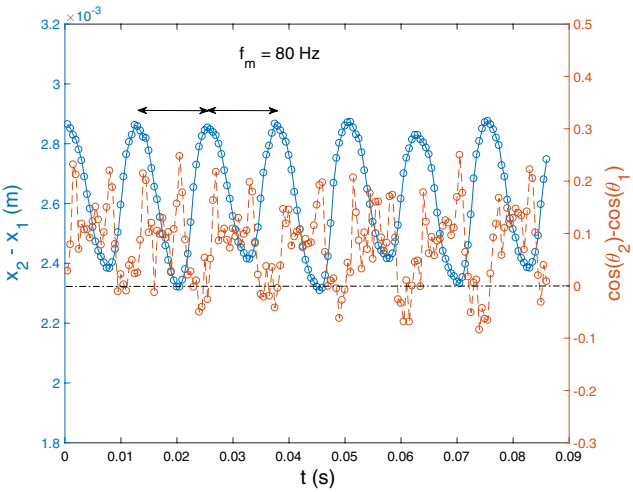
f_m = 80 Hz
x_2 - x_1 (m)
cos(θ_2)-cos(θ_1)
t (s)

(d)

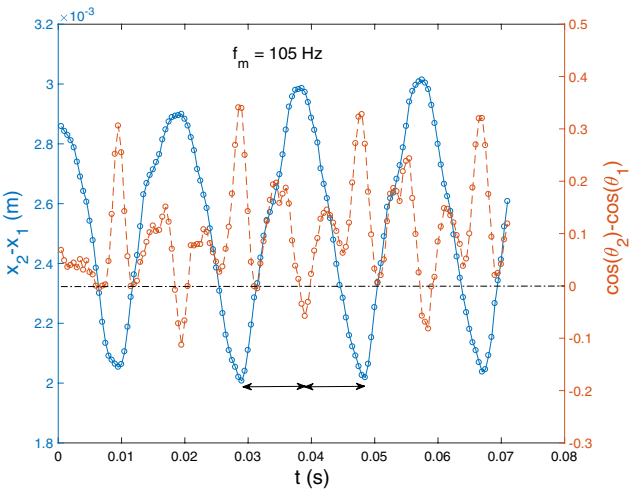
f_m = 105 Hz
x_2-x_1 (m)
cos(θ_2)-cos(θ_1)
t (s)

(e)

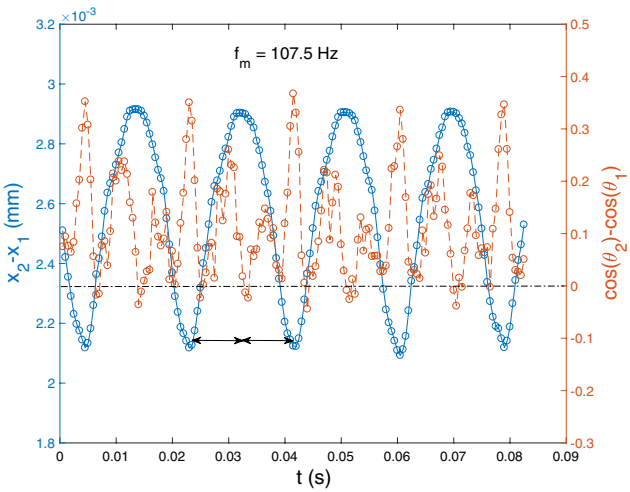
f_m = 107.5 Hz
x_2-x_1 (mm)
cos(θ_2)-cos(θ_1)
t (s)

(f)

◂**Fig. 6** Basal radius ($x_2 - x_1$) (blue circles, plain line, left axis) and cosine difference ($\cos\theta_2 - \cos\theta_1$) (red circles, dashed line, right axis) versus time for different modulation frequencies and $d = 1.38$ nm. **a** $f_m = 30$ Hz, **b** $f_m = 40$ Hz, **c** $f_m = 55$ Hz, **d** $f_m = 80$ Hz, **e** $f_m = 105$ Hz, **f** $f_m = 107.5$ Hz. The double arrows show the time interval $1/f_m$ and evidence a drop response with period-doubling for (**d**, **e**, **f**), harmonic for (**c**), quasi-harmonic for (**b**) and aperiodic for (**a**)

natural frequency of oscillations exhibited by the drop in the absence of modulation. In particular, when f_m is taken close to the harmonic or parametric resonances of the drop (here, respectively, near 50 and 100 Hz), one measures a significant increase of the amplitude of CL oscillations and of the averaged velocity, which can find its origin in the time evolution of the CLs velocity and CAs.

Our results show oscillating CLs with $\mathrm{Ca}_i(\theta_i)$ which does not follow the classical Cox–Voinov hydrodynamics theory of wetting. This is reminiscent of measurements on vibrating drops or menisci (Brunet et al. 2007; Costalonga and Brunet 2020; Ting and Perlin 1995; Jiang et al. 2004) and suggests that there is a missing ingredient to be added to the classical hydrodynamic theory. Some of these theories include inertia in dynamical wetting equations (Cox 1998; Hocking and Davis 2002), but are non-adapted to our situation, where the inner flow is rather complex and which details remain unknown. Previous experiments on drops or menisci subjected to slanted vibrations (Brunet et al. 2007; Costalonga and Brunet 2020; Ting and Perlin 1995; Jiang et al. 2004) already pointed out this indetermination in the relation $\mathrm{Ca}_i(\theta_i)$. Some attempts to better quantify this behaviour were proposed either by extracting a phase shift between symmetric and asymmetric modes (Costalonga and Brunet 2020; Sartori et al. 2015, 2019), or by prescribing ad hoc relationships with non-single-valued $\mathrm{Ca}_i(\theta_i)$ in a more global model (Bradshaw and Billingham 2018; Miles 1990). Our own attempts to treat our data by quantifying this phase shift remain partly conclusive. From time series of $(\cos\theta_2 - \cos\theta_1)$ and $x_2 - x_1$, we were able to explain the most obvious situations, i.e. where the most pronounced asymmetry occurs at the same phase as the smallest basal radius and corresponds to the largest values of averaged velocity (see Fig. 6). But some important points remain ill-explained. In particular, a significant difference of our results with aforementioned experiments on mechanically vibrated drops is that the averaged velocity is not related to the averaged motile force given by Eq.(5), see Fig. 4-(a). From plots of Ca_i versus θ_i (Figures 7), the optimum of the drop mobility (maximal averaged Ca) corresponds either to the occurrence of a large loop in the advancing phase (harmonic resonance near 50 Hz), either by multiple narrower and less defined loops, or by a shift of values between the left and right sides of the drop (aperiodic responses or parametric resonance near 100 Hz). What can be stated in a qualitative level is that a relatively simple dynamics of the drop CL (harmonic response) corresponds to a single loop in $\mathrm{Ca}_i(\theta_i)$ plots and that a more complex response (for instance aperiodic or period-doubling) tends to create narrower and more complex sets of loops in the corresponding plots.

A possible framework to better quantify the relationship between dynamical angle and velocity in oscillating CLs was recently proposed by Xia and Steen (2018, 2020). However, it requires a reference (fixed) position for the contact line, which in our situation is hard to define due to the net motion of the drop. Our attempts to apply this framework with a time-drifting reference position did not give any convincing trends.

What also remains to be quantified is the range of dynamical CA θ_i in which the CL remains pinned. Although some qualitative trends can be extracted from plots Ca_i versus θ_i too (Fig. 7), which would suggest that the range of hysteresis is velocity-dependent similarly to previous vibrating CL experiments (Johnson and Dettre 1964; Andrieu et al. 1994; Decker and Garoff 1996; Della Volpe et al. 2002), there is no neat dependence of the effective onset of CL motion or in CA hysteresis on ΔR (see Fig. 4-(b)). Still, this hypothesis can be based on physical grounds, as it was recently shown by thorough experiments on low-hysteresis substrates that both the macroscopic and microscopic equilibrium angles should be velocity-dependent (Perrin et al. 2016).

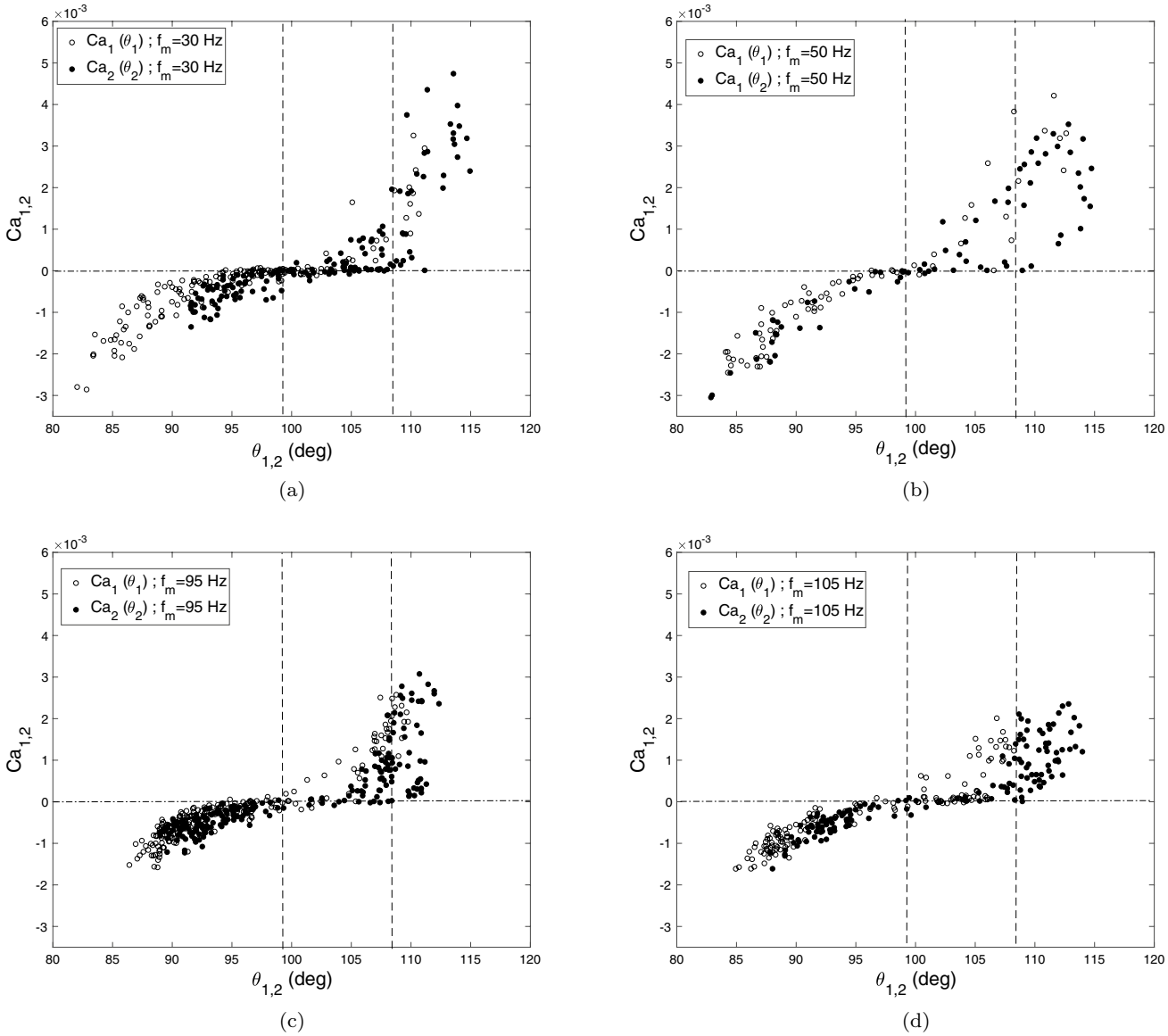

Fig. 7 Relationship between dynamical CA and dimensionless CL velocity at the rear/left (index 1, open symbols) and front/right (index 2, filled symbols) for a 7.5 μl drop excited by 19.7 MHz SAWs, with $d = 1.38$ nm and modulated at **a** $f_m = 30$ Hz, **b** $f_m = 50$ Hz, **c** $f_m = 95$ Hz, **d** $f_m = 105$ Hz. The dashed line indicates Ca = 0, while the two dashed-dotted lines indicate θ_R and θ_A

In more applied prospectives, the low-frequency-modulated SAWs have proven to be an efficient way to move droplets on inclines (Bussonniere et al. 2021). This encouraging result could be extended on substrates with stronger CA hysteresis.

Acknowledgements We thank Maxime Costalonga for his help in data treatment.

References

Alghane M, Fu YQ, Chen BX, Li Y, Desmulliez MPY, Walton AJ (2012) Frequency effect on streaming phenomenon induced by Rayleigh surface acoustic wave in microdroplets. J Appl Phys 112:084902

Andrieu C, Sykes C, Brochard F (1994) Average spreading parameter on heterogeneous surfaces. Langmuir 10:2077–2080

Baudoin M, Brunet P, Bou Matar O, Herth E (2012) Low power sessile droplets actuation via modulated surface acoustic waves. Appl Phys Lett 100:154102

Bonn D, Eggers J, Indekeu J, Meunier J, Rolley E (2009) Wetting and spreading. Rev Mod Phys 81:739–805

Bostwick JB, Steen PH (2009) Capillary oscillations of a constrained liquid drop. Phys Fluids 21:032108
Bostwick J. B, Steen PH (2014) Dynamics of sessile drops. Part 1. Inviscid theory. J Fluid Mech 760:5–38
Bradshaw JT, Billingham J (2018) Thick drops climbing uphill on an oscillating substrate. J Fluid Mech 840:131–153
Brunet P, Eggers J, Deegan RD (2007) Vibration-induced climbing of drops. Phys Rev Lett 99:144501
Brunet P, Baudoin M, Bou-Matar O, Zouesthiagh F (2010) Droplets displacement and oscillations induced by ultrasonic surface acoustic waves: a quantitative study. Phys Rev E 81:036315
Burgmann S, Dues M, Barwari B, Steinbock J, Bttner L, Czarske J, Janoske U (2021) Flow measurements in the wake of an adhering and oscillating droplet using laser Doppler velocity profile sensor. Exp Fluids 62:47
Bussonniere A, Baudoin M, Brunet P, Bou Matar O (2016) Dynamics of sessile and pendant drops excited by surface acoustic waves: gravity effects and correlation between oscillatory and translational motions. Phys Rev E 93:053106
Bussonniere A, Bou Matar-Lacaze O, Baudoin M, Brunet P (2021) Method for increasing the ability of at least one droplet to slide over a medium, US Patent 11,090,698
Celestini F, Kofman R (2006) Vibration of submillimeter-size supported droplets Phys. Rev E 73:041602
Chang CT, Bostwick JB, Daniel S, Steen PH (2015) Dynamics of sessile drops. Part 2. Experiment. J Fluid Mech 768:442–467
Chastrette N, Baudoin M, Brunet P, Royon L, Wunenburger R (2021) Elucidating the oscillation instability of sessile drops triggered by surface acoustic waves, Submitted
Chu B-T, Apfel RE (1982) Acoustic radiation pressure produced by a beam of sound. J Acoust Soc Am 72:1673–1687
Cinbis C, Mansour NN, Khuri-Yakub BT (1993) Effect of surface tension on the acoustic radiation pressure-induced motion of the water-air interface. J Acoust Soc Am 94:2365–2372
Connacher W, Orosco J, Friend JR (2020) Droplet ejection at controlled angles via acoustofluidic jetting. Phys Rev Lett 125:184504
Costalonga M, Brunet P (2020) Directional motion of vibrated sessile drops: a quantitative study. Phys Rev Fluids 5:023601
Cox RG (1998) Inertial and viscous effects on dynamic contact angles. J Fluid Mech 357:249–278
Decker EL, Garoff S (1996) Using vibrational noise to probe energy barriers producing contact angle hysteresis. Langmuir 12:2100–2110
Della Volpe C, Maniglio D, Morra M, Soboni S (2002) The determination of a ÔstableequilibriumÕ contact angle on heterogeneous and rough surfaces. Colloids Surf A 206:47–67
Dentry MB, Yeo LY, Friend JR (2014) Frequency effects on the scale and behavior of acoustic streaming. Phys Rev E 89:013203
Dimitrakopoulos P, Higdon JJL (1998) On the displacement of three-dimensional fluid droplets from solid surfaces in low-Reynolds-number shear flows. J Fluid Mech 377:189–222
Dussan VEB (1979) On the spreading of liquids on solid surfaces: static and dynamic contact lines. Annu Rev Fluid Mech 11:371–400
Eddi A, Winkels KG, Snoeijer JH (2013) Influence of droplet geometry on the coalescence of low viscosity drops. Phys Rev Lett 111:144502
Elrod SA, Hadimioglu B, Khuri-Yakub BT, Rawson EG, Richley E, Quate CF, Mansour NN, Lundgren TS (1989) Nozzleless droplet formation with focused acoustic beams. J Appl Phys 65:3441–3447
Fayzrakhmanova IS, Straube AV (2009) Stick-slip dynamics of an oscillated sessile drop. Phys Fluids 21:072104
Friend JR, Yeo LY (2011) Microscale acoustofluidics: microfluidics driven via acoustics and ultrasonics. Rev Modern Phys 83:647
Guo YJ, Lv HB, Li YF et al (2014) High frequency microfluidic performance of LiNbO3 and ZnO surface acoustic wave devices. J Appl Phys 116:024501
Hocking LM (1987) Waves produced by a vertically oscillating plate. J Fluid Mech 179:267–281
Hocking LM, Davis SH (2002) Inertial effects in time-dependent motion of thin films. J Fluid Mech 467:1–17
Hodgson G, Passmore M, Skarysz M, Garmory A, Paolillo F (2021) Contact angle measurements for automotive exterior water management. Exp Fluids 62:119
Insepov Z, Ramazanova Z, Zhakiyev N, Tynyshtykbayev K (2021) Water droplet motion under the influence of Surface Acoustic Waves (SAW). J Phys Commun 5:035009
Issenmann B, Nicolas A, Wunenburger R, Manneville S, Delville J-P (2008) Deformation of acoustically transparent fluid interfaces by the acoustic radiation pressure. Europhys Lett 83:34002
Jiang L, Perlin M, Schultz WW (2004) Contact-line dynamics and damping for oscillatory free surface flows. Phys Fluids 16:748–758
Johnson RE, Dettre RH (1964) Contact angle hysteresis. Adv Chem Ser 43:112–135
Lamb H (1932) Hydrodynamics. Cambridge University Press, Cambridge, England
Le Grand N, Daerr A, Limat L (2005) Shape and motion of drops sliding down an inclined plane. J Fluid Mech 541:293
Lei Y, Hu H (2020) SAW-driven droplet jetting technology in microfluidic: a review. Biomicrofluidics 14:061505
Li F, Mugele F (2008) How to make sticky surfaces slippery: contact angle hysteresis in electrowetting with alternating voltage. Appl Phys Lett 92:244108
Long J, Chen P (2006) On the role of energy barriers in determining contact angle hysteresis. Adv Coll Interf Sci 127:55–66
Miles JW (1990) Capillary-viscous forcing of surface waves. J Fluid Mech 219:635–646
Noblin X, Buguin A, Brochard-Wyart F (2004) Vibrated sessile drops: transition between pinned and mobile contact line oscillations. Eur Phys J E 14:395–404
Noblin X, Kofman R, Celestini F (2009) Ratchetlike Motion of a Shaken Dro. Phys Rev Lett 102:194504
Perrin H, Lhermerout R, Davitt K, Rolley E, Andreotti B (2016) Defects at the nanoscale impact contact line motion at all scales. Phys Rev Lett 116:184502
Perrin H, Lhermerout R, Davitt K, Rolley E, Andreotti B (2018) Thermally activated motion of a contact line over defects. Soft Matter 14:1581–1595
Petrov J. G, Ralston J, Schneemilch M, Hayes RA (2003) Dynamics of Partial Wetting and Dewetting in Well-Defined Systems. J Phys Chem B 107:1634–1645
Puthenveettil BA, Senthilkumar VK, Hopfinger EJ (2013) Motion of drops on inclined surfaces in the inertial regime. J Fluid Mech 726:26–61
Riaud A, Baudoin M, Bou Matar O, Thomas J.-L., Brunet P (2017) On the influence of viscosity and caustics on acoustic streaming in sessile droplets: an experimental and a numerical study with a cost-effective method. J Fluid Mech 821:384–420
Sartori P, Quagliati D, Varagnolo S, Pierno M, Mistura G, Magaletti F, Casciola CM (2015) Drop motion induced by vertical vibrations. New J Phys 17:113017
Sartori P, Guglielmin E, Ferraro D, Filippi D, Zaltron A, Pierno M, Mistura G (2019) Motion of Newtonian drops deposited on liquid-impregnated surfaces induced by vertical vibrations. J Fluid Mech 876:R4

Sharp JS (2012) Resonant properties of sessile droplets; contact angle dependence of the resonant frequency and width in glycerol/water mixtures. Soft Matter 8:399–407
Shilton RJ, Travagliati M, Beltram F, Cecchini M (2014) Nanoliter-Droplet acoustic streaming via ultra high surface acoustic waves. Adv Mat 26:4941–4946
Sikalo S, Tropea C, Ganic EN (2005) Dynamic wetting angle of a spreading droplet. Exp Thermal Fluid Sci 29:795–802
Snoeijer JH, Andreotti B (2013) Moving contact lines: scales, regimes and dynamical transitions. Ann Rev Fluid Mech 45:269–292
Steen PH, Chang CT, Bostwick JB (2019) Droplet motions fill a periodic table. Proc Natl Acad Sci 116:4849–4854
Strani M, Sabetta F (1984) Free vibrations of a drop in partial contact with a solid support. J Fluid Mech 141:233
Ting C-L, Perlin M (1995) Boundary conditions in the vicinity of the contact line at a vertically oscillating upright plate: an experimental investigation. J Fluid Mech 295:263–300
Tsamopoulos J, Brown R (1983) Nonlinear oscillations of inviscid drops and bubbles. J Fluid Mech 127:519
Voinov OV (1976) Hydrodynamics of wetting. Fluid Dyn 11:714–721
Xia Y, Steen PH (2018) Moving contact-line mobility measured. J. Fluid Mech. 841:767–783
Xia Y, Steen P. H (2020) Dissipation of oscillatory contact lines using resonant mode scanning. NPJ Microgravity

Authors and Affiliations

P. Brunet[1] · **M. Baudoin**[2]

[1] Laboratoire Matière et Systèmes Complexes, UMR CNRS 7057, Université Paris Diderot, 10 rue Alice Domon et Léonie Duquet, 75205 Paris cedex 13, France

[2] Univ. Lille, CNRS, Centrale Lille, Univ. Polytechnique Hauts-de-France, UMR 8520 - IEMN - Institut d'Electronique de Microélectronique et de Nanotechnologie, F-59000 Lille, France